Acta Biomaterialia 163 (2023) 131–145

Contents lists available at ScienceDirect

Acta Biomaterialia

journal homepage: www.elsevier.com/locate/actbio

Full length article

Changes in elastin structure and extensibility induced by hypercalcemia and hyperglycemia☆

Chengeng Yang[a], Anthony S. Weiss[b,c,d], Anna Tarakanova[a,e,*]

[a] Department of Biomedical Engineering, University of Connecticut, Storrs, CT, USA
[b] Charles Perkins Centre, The University of Sydney, Sydney, NSW, Australia
[c] School of Life and Environmental Sciences, The University of Sydney, Sydney, NSW, Australia
[d] Sydney Nano Institute, The University of Sydney, Sydney, NSW, Australia
[e] Department of Mechanical Engineering, University of Connecticut, Storrs, CT, USA

ARTICLE INFO

Article history:
Received 15 December 2021
Revised 17 March 2022
Accepted 24 March 2022
Available online 30 March 2022

Keywords:
Tropoelastin
Hyperglycemia
Hypercalcemia
Aging
Molecular dynamics
Biomechanics

ABSTRACT

Elastin is a key elastomeric protein responsible for the elasticity of many organs, including heart, skin, and blood vessels. Due to its intrinsic long life and low turnover rate, damage in elastin induced by pathophysiological conditions, such as hypercalcemia and hyperglycemia, accumulates during biological aging and in aging-associated diseases, such as diabetes mellitus and atherosclerosis. Prior studies have shown that calcification induced by hypercalcemia deteriorates the function of aortic tissues. Glycation of elastin is triggered by hyperglycemia and associated with elastic tissue damage and loss of mechanical functions via the accumulation of advanced glycation end products. To evaluate the effects on elastin's structural conformations and elasticity by hypercalcemia and hyperglycemia at the molecular scale, we perform classical atomistic and steered molecular dynamics simulations on tropoelastin, the soluble precursor of elastin, under different conditions. We characterize the interaction sites of glucose and calcium and associated structural conformational changes. Additionally, we find that elevated levels of calcium ions and glucose hinder the extensibility of tropoelastin by rearranging structural domains and altering hydrogen bonding patterns, respectively. Overall, our investigation helps to reveal the behavior of tropoelastin and the biomechanics of elastin biomaterials in these physiological environments.

Statement of significance

Elastin is a key component of elastic fibers which endow many important tissues and organs, from arteries and veins, to skin and heart, with strength and elasticity. During aging and aging-associated diseases, such as diabetes mellitus and atherosclerosis, physicochemical stressors, including hypercalcemia and hyperglycemia, induce accumulated irreversible damage in elastin, and consequently alter mechanical function. Yet, molecular mechanisms associated with these processes are still poorly understood. Here, we present the first study on how these changes in elastin structure and extensibility are induced by hypercalcemia and hyperglycemia at the molecular scale, revealing the essential roles that calcium and glucose play in triggering structural alterations and mechanical stiffness. Our findings yield critical insights into the first steps of hypercalcemia- and hyperglycemia-mediated aging.

1. Introduction

As one of the essential components in the extracellular matrix, elastin fibers feature primarily in providing support and elasticity to various tissues and organs, from arterial walls to lung, skin, and heart [1]. Elastin, the dominant component of elastic fibers, is assembled from its subunit monomer, tropoelastin, whereby tropoelastin monomers undergo coacervation, extensive intra- and intermolecular cross-linking, and eventually incorporation into elastic fibers [2].

Abbreviations: RMSF, Root mean square fluctuation; SASA, solvent accessible surface area; Rg, radius of gyration; NEP, neprilysin; PE, pancreatic elastase; WT, wild type.

☆ Part of the Special Issue on the Mechanics of Cells and Fibers, guest-edited by Professors Amrinder S. Nain, Derrick Dean, and Guy M. Genin.

* Corresponding author.
E-mail address: anna.tarakanova@uconn.edu (A. Tarakanova).

https://doi.org/10.1016/j.actbio.2022.03.041
1742-7061/

Over time, dermal, cardiovascular, and pulmonary tissues become increasingly stiff and less able to recoil with age, leading to the hypothesis that age-related failure of elastic fibers may dictate the apparent 100-120-year limit on human life expectancy [3,4]. With a low turn-over rate during its long life, elastin is highly susceptible to cumulative effects of biochemical damage [4]. Biological aging, as well as many age-related chronic diseases, including diabetes, atherosclerosis, and arthritis are characterized by an imbalance in the biochemical environment, which accelerates the rate of elastic tissue degradation and associated changes to mechanical function [5–7]. Calcium, one of the most prevalent elements in the body, is an important component of teeth and bones, yet it is also involved in aging diseases, such as medial elastocalcinosis, the calcification in the tunica media of vascular walls, and atherosclerosis, where vascular structures and functions are significantly impaired [8,9]. Glucose, an important source of energy in the body, is also linked to aging-related diseases affecting elastic tissues. For instance, glycation of protein induced by glycemia leads to alterations of mechanical properties in the vasculature, as observed in diabetic patients [8,10]. Such aging-linked environmental factors, however, are intrinsic and unavoidable in the body because calcium ions and glucose are abundant in the diet and required for normal biological processes [8]. Therefore, it is prudent to investigate the underlying damage mechanisms associated with hyperglycemia and hypercalcemia, in order to specifically target and prevent aging-related diseases, than eliminate these factors from the body. Calcification, as commonly observed pathologically in the tunica media of vascular walls [11], is a pervasive process, where calcium phosphate binds to and deposits on the elastin protein, stimulating smooth muscle cells to express bone mineralization proteins that are normally expressed by osteocytes [12]. Consequently, minerals nucleate along the elastin lamellae [13] and grow unregulated in the extracellular matrix (ECM) [14], impairing the biological function of elastic tissues, particularly in the elastin-rich vasculature [15], yielding further stiffening of arterial walls [11], higher values of systolic pressure, and ultimately increasing the incidence of cardiovascular events [8,15–17]. Additionally, increasing evidence indicates that hyperglycemia, the elevated glucose level in the blood, is a significant initiating cause of tissue damage and loss of mechanical function occurring in aging and diabetes, either through repeated acute changes in cellular glucose metabolism, or through the long-term accumulation of glycated biomolecules and advanced glycation end products (AGEs) [8,18–20]. AGEs are formed by a series of successive chemical reactions between a reducing sugar, such as glucose, and a protein or lipid. Unlike functionality-inferring enzymatic crosslinks, AGEs are pathological and alter the biochemical equilibrium and mechanical performance of tissues [21,22]. Furthermore, it has been reported that the presence of glucose and AGEs enhances adsorption of calcium ions and precipitates calcification, which is attributed to stiffening and loss of function in aortic elastic tissue [17,23,24]. Apart from the accelerating effects by AGEs on mineral deposition, a positive correlation was also reported between the fragmentation level of elastin fibers and the extent of vascular calcification [12,25]. Despite their significant roles in aging and disease, there exists neither an exhaustive investigation on the fundamental mechanisms of how calcium ions and glucose interact with elastin, nor comprehensive studies to characterize the effects of calcification and non-enzymatic glycation modifications on the atomistic structure and mechanical properties of elastin, due to the complicated disordered nature of elastin's tertiary structure formed in coacervation, cross-linking and assembly. To our best knowledge, we present here the first study to offer structural, conformational and mechanistic insights into the influence of calcium ions, glucose, and their cooperative effects on elastin at the molecular scale.

Recently, molecular dynamics (MD) simulations have been widely used in molecular biology [26]. As a well-established complementary method to experimental approaches, it provides a feasible means to investigate and predict many biological processes, including protein folding, ligand binding and stress-induced displacement at the atomistic scale [26]. Previously, the fully atomistic model of tropoelastin, the soluble precursor of elastin protein, was revealed by means of replica exchange MD simulations [25,27], identifying that tropoelastin retains a defined structure but at the same time paradoxically displays a large portion of flexible, disordered regions needed for elasticity [28], represented by an ensemble of elastic conformers. To investigate the variations of structural conformations of elastin in the presence of elevated glucose and calcium ions levels at the molecular level, we implemented the same atomistic model of tropoelastin in microsecond classical MD simulations in the present study. As tropoelastin's central domains are believed to be chiefly involved in biomechanical functions [25,27,28], to evaluate the effects of hyperglycemia and hypercalcemia on elastin mechanics, we performed tensile simulations on the central domains of tropoelastin under different conditions, examining the changes in mechanical response and structural characteristics.

We find that calcium binding triggers structural collapse of the monomer, rendering a more compact and ordered global structure, and introduces multi-phase stiffness in the mechanical properties. The binding of glucose tends to disrupt ordered local secondary structures by replacing hydration waters and forming hydrogen bonds with the protein, and results in increased fluctuations, a loosely formed structure, and an increased modulus of elasticity. We also investigated the coupling effects of calcium ions and glucose by fixing the concentration of one substance and varying the other. Interestingly, due to the opposite influence by calcium ions and glucose on the molecular motions, the protein shows a nonlinear tendency with the increment of one substance with the other constant. This observation is consistent with the highly flexible nature of elastin, suggesting that elastin is substantially sensitive to physiochemical stressors. Overall, our investigation helps to reveal the molecular behavior of elastin in complex physiological environments and informs possible molecular mechanisms of aging in elastic tissues.

2. Materials and methods

2.1. Molecular dynamics simulations of monomeric elastin

The starting structure of tropoelastin was chosen from our previous work based on human tropoelastin isoform 2 [25], where the molecule has been well equilibrated by REMD simulations. Atomistic classical MD simulation of wild type (WT) tropoelastin in a water box of $15 \times 15 \times 15$ nm^3 was performed using the Gromacs simulation package [29], version 2021.2, at 27°C, for a total running time of 1000 ns. Simulations of tropoelastin with 1000 mM calcium ions and/or 1969 mM glucose were performed at the same temperature. We investigate these two edge cases by introducing 1000 mM calcium and 1969 mM glucose, respectively, both of which reach the saturated concentration in the water box, to investigate specific individual influence by calcium ions and glucose on tropoelastin. To elucidate the coupling effects of calcium ions and glucose, we reduced the calcium concentration to 750 mM to accommodate glucose, with a concentration range from 62.5 mM, 123 mM, 185 mM to 246 mM. Similarly, we reduced the glucose concentration to 738 mM to accommodate calcium ions, with a concentration range from 100 mM, 200 mM, 300 mM to 400 mM. Both calcium ions and glucose molecules were introduced with different random seed numbers in each different condition, therefore, their initial configurations were randomized in each condition.

Topology and force field parameters were assigned from the CHARMM36m [30] protein parameter set for elastin and from the CHARMM36 [30] sugar parameter set for α-D-glucose. We also used CHARMM36 [30] force field to introduce calcium. The TIP3P model was used for water molecules [31]. The Particle Mesh Ewald (PME) method was used for computing electrostatic forces with grid spacing of 1.6 Å [32]. The short-range electrostatic interactions and Lennard-Jones interactions were calculated using a cut-off radius of 12 Å, and long-range dispersion corrections were applied for energy and pressure. The whole system was first energy minimized by the steepest descent algorithm with aforementioned distance restraints for a maximum of 50,000 steps. After minimization, short 100 ps temperature and pressure equilibration runs were performed in NVT and NPT ensembles, respectively. The V-rescale thermostat was used for temperature coupling [33], where both protein and non-protein groups were coupled to separate temperature baths of 300 K (27°C), with 0.1 ps as the time constant; and the Parrinello Rahman barostat [34] for pressure coupling, where isotropic pressure coupling was selected with 2 ps as the time constant, 1 bar as the reference pressure, and $4.5e^{-5}$ bar^{-1} as compressibility. Also, the center of mass of the reference coordinates was scaled with the scaling matrix of the pressure coupling during pressure equilibration. The leap-frog algorithm [35] was applied with an integration time step of 1 fs for initial equilibration and 2 fs for MD production runs. The position restraint was implemented on heavy atoms by setting -DPOSRES as the parameter for "define", the LINCS algorithm [36] was used to constrain covalent bonds with hydrogen atoms and the aforementioned distance restraints and long-range dispersion corrections were applied in both temperature and pressure equilibration runs. After initial equilibration, the position restraint on heavy atoms was removed, and 1000 ns production runs were performed in the NPT ensemble with bond constraints with LINCS [36] and the aforementioned distance restraints and long-range dispersion corrections.

2.2. Steered molecular dynamics simulations of monomeric elastin domains

Domains 10-19 of tropoelastin were spliced from the same starting structure of the whole molecule to perform steered MD simulations, as these domains are chiefly involved in elastin's elasticity. These domains were placed in a water box of $10 \times 10 \times 160$ nm^3 in 27°C using the Gromacs simulation package [29], version 2018.3 for a total running time of 3.5 ns. The α-carbon of the last residue in domain 19 was fixed, and the α-carbon of the first residue in domain 10 was pulled at a velocity of 50 m/s and a force constant of 1000 kJ mol^{-1} nm^{-2} along the axis parallel to the length of the molecule. To investigate the specific role that calcium ions and glucose play in altering mechanical properties of tropoelastin and the correlation between such variations and calcium/glucose concentrations, we introduced calcium ions with a concentration range of 100 mM, 750 mM, 1000 mM, 1500 mM to 2000 mM, to represent hypercalcemia, and glucose with a concentration range of 246 mM, 493 mM, 738 mM, 985 mM to 1969 mM, to represent hyperglycemia, with tropoelastin only as the control. We set up three replicates for each condition. To study the coupling effects of calcium and glucose on mechanical profiles, we added 750 mM of calcium with glucose ranging from 62.5 mM to 246 mM as respective cases; we also fixed glucose concentration at 738 mM while ranging calcium concentrations from 100 mM to 400 mM. Each condition also has three replicates, and the pulling forces and strains were calculated based on these replicates for each condition.

Similar topology, force field parameters, coupling methods, and algorithms were used for steered MD simulations, except for an additional temperature equilibration that was performed using the NVT ensemble with V-rescale temperature coupling [33] after the two aforementioned equilibrations, for 200 ps with the same parameter setting as the first NVT ensemble except position restraints excluded on the protein. A leap-frog algorithm was applied with an integration time step of 1 fs for equilibration and 2 fs for steered MD simulation [35]. After equilibration, new velocities were generated from the Maxwell distribution and Nose-Hoover [37] was chosen for temperature coupling, in subsequent steered MD simulations.

2.3. Data analysis

All simulation trajectories were processed using in-house and Gromacs scripts [29]. Visualization was performed in VMD [38]. Analysis of root mean square fluctuation (RMSF) and pulling forces during the whole trajectory were conducted using Gromacs and in-house scripts. Analysis of hydrogen bonds, solvent accessible surface area (SASA), secondary structures, radius of gyration (Rg) were conducted using Gromacs and sampled for the last 100 ns of the trajectory for averaging. For secondary structure analysis, the DSSP algorithm [39] was used; all types of helices were assigned as helices, and all β-structures, including β-sheets and β-bridges, were assigned as betas. Salt bridge analysis was conducted using the VMD plugin [38]. Contact maps, hydration water calculations, and strain calculations were based on in-house scripts with the aid of the MDAnalysis python library [40,41].

3. Results

3.1. Calcium binding effects on elastin structure and mechanical properties

3.1.1. Calcium-bound domains show reduced local fluctuation and altered structure

Schematic representation of tropoelastin structure is depicted in Fig. S1 to show domain arrangement. Structural variations and motion variability of WT tropoelastin in 1000 mM calcium was analyzed (Fig. 1). We find four recurring binding sites of calcium ions, all of which occur at negatively charged residues: aspartate (D)72 in domain 6, glutamate (E)345 in domain 19, glutamate (E)414 in domain 21 and C-terminal lysine (K)698 in domain 36. Snapshots of time-wise representative structures and each binding pocket are detailed in Fig. 1A (i) - (ii), respectively. Interestingly, D72 binds two calcium ions while others only bind one calcium ion. Such binding reduces local fluctuation as measured by residue-wise root mean square fluctuation (RMSF) (Fig. 1B) and alters local secondary structure distributions (Fig. S2A (i)-(iv)). The RMSF pattern suggests an overall reduction in flexibility compared with the control, except for slight increments at residues 130-148 largely corresponding to domain 10, residues 264-326 corresponding to domains 17-18, and residues 373-383 in domain 20. Compared to the control with no salt added, the binding of calcium ions induces a decrease of bend and turn structures, but increases helices and coils in domain 6; in domain 19, the helices are transformed into coils and turns; in domain 21, a 4.5% decrement in helices and 4% increment in turns are observed; in domain 36, H-bonded bends are converted into flexible coil structures. Globally, we find more ordered secondary structures, e.g., an increase in helices, and reduction of disordered secondary structures such as coils (Fig. 1C).

The negatively charged residues in tropoelastin feature in forming salt bridges with nearby positively charged groups, commonly, lysines and arginines. Compared to the control where stable salt bridges exist between D72 and K78, with other transient ones between E345 and K289, E345 and K349, E345 and K356, E414 and

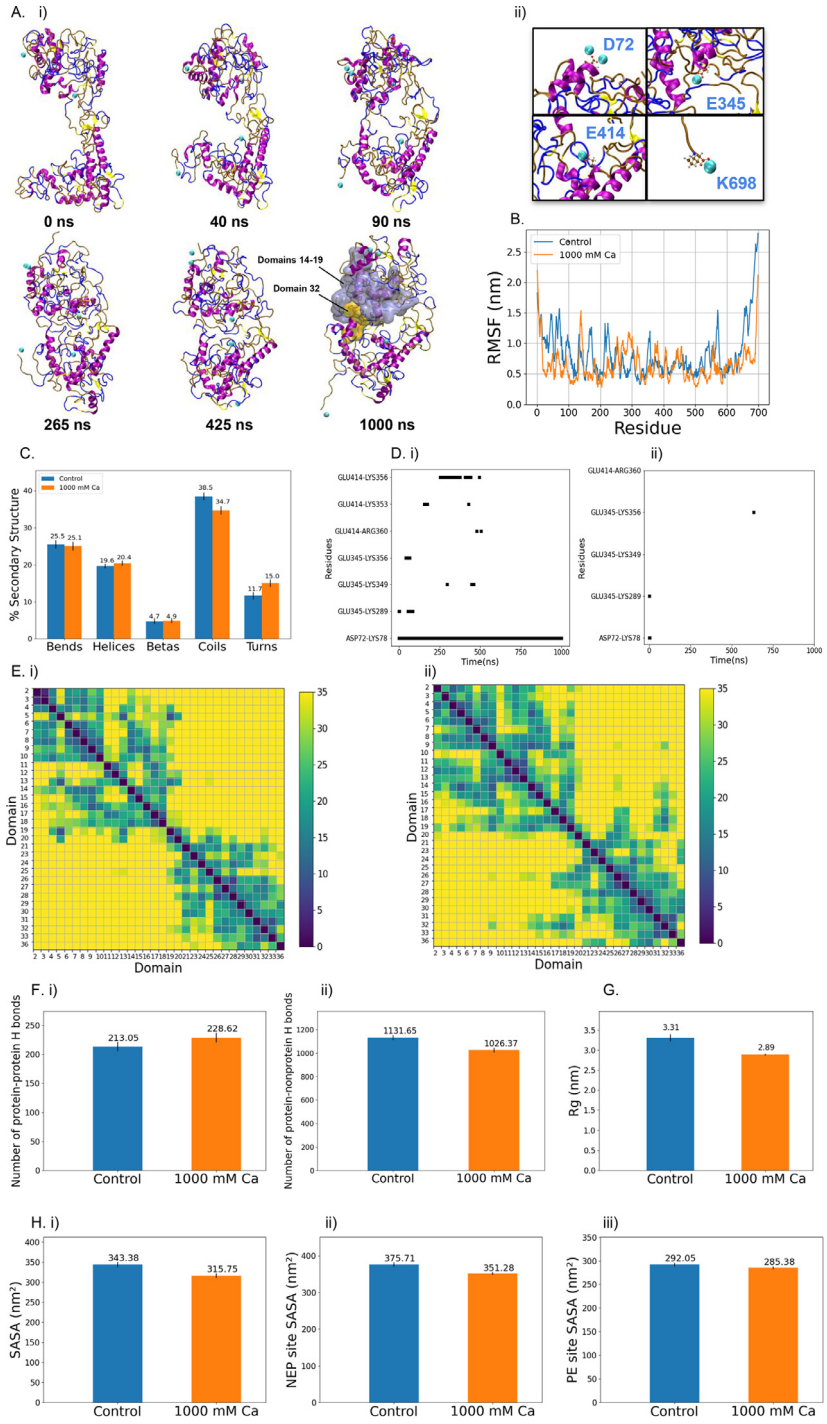

Fig. 1. Calcium effects on tropoelastin structure
(A, i) Representative structures of tropoelastin + 1000 mM calcium (ii) snapshots of four binding pockets.
(B) Root mean square fluctuation (RMSF) of control and tropoelastin + 1000 mM calcium ions.
(C) Global secondary structure of control and tropoelastin + 1000 mM calcium ions in the last 100 ns of simulation.
(D) Salt bridge presence and longevity of (i) control and (ii) tropoelastin + 1000 mM calcium ions.
(E) Residue-wise contact maps with a cut-off distance of 35 A showing intramolecular interactions in (i) control and (ii) tropoelastin + 1000 mM calcium ions in the last 100 ns of simulation.
(F) Hydrogen bonding within the control and tropoelastin + 1000 mM calcium ions for (i) intramolecular bonding and (ii) bonding between protein and water in the last 100 ns of simulation.
(G) Radius of gyration (Rg) of control and tropoelastin + 1000 mM calcium ions in the last 100 ns of simulation.
(H) Solvent accessible surface area (SASA) of control and tropoelastin + 1000 mM calcium ions for (i) the whole molecule, (ii) cleavage sites by neprilysin and (iii) cleavage sites by pancreatic elastase in the last 100 ns of simulation.

R360, E414 and K353, and K414 and K356 (Fig. 1D (i)), the introduction of calcium ions apparently disrupts these intramolecular salt bridges (Fig. 1D (ii)), due to their more robust positive electric charge compared with lysines. Overall, these findings suggest that calcium binding contributes to reduction in local fluctuation, more ordered secondary structures, and disruption of salt bridges.

3.1.2. Calcium binding promotes altered dynamic behavior and structural collapse globally

We find that the binding of calcium ions introduces significant variations in molecular motions globally. Snapshots of representative structures depict this time-wise mobility (Fig. 1A (i)). Unlike the motions of the control characterized by twisting at the N-terminus region and scissors-like bending in the C-terminus regions [27], tropoelastin with added 1000 mM calcium shows a tendency toward structural collapse, where domain 32 tends to move upward to the vicinity of domains 14 and 15, the N-terminus destabilizes, and domain 18 and 19 transition downward to contact domain 32. Domain 32 is observed to be trapped inside the pocket formed by domains 14-19. The residue-wise contact map showing average intramolecular contacts in the last 100 ns of simulation also reflects this tendency (Fig. 1E (i)-(ii)). Other increased intramolecular contacts among domains are mainly found in domain 5 with domains 2-3, domains 26-27 with domains 17-18, domains 11-12 with domains 2-6, and domain 36 with domains 21-24; while contacts among the following domains are found to be diminished, namely between domain 10 with domains 2-8, domain 17 with domains 14-15, and domain 7 with domain 2. These observations of intramolecular contacts imply a rearrangement of tropoelastin domains and may be responsible for changes in elastin functionality, including a stiffened mechanical response.

The altered molecular fluctuations and structural collapse of the molecule with the addition of calcium ions is accompanied by a reduced number of hydrogen bonds formed between protein and water, yet enhanced hydrogen bonds within the protein (Fig. 1F (i)-(ii)). We also examine the solvent accessible surface area (SASA) (Fig. 1G (i)) and radius of gyration (Rg) (Fig. 1H) of the whole molecule, finding an enhanced buried molecular surface area and a more compact global structure that is consistent with more hydrogen bonding within protein in the presence of calcium ions, induced by calcium-binding mediated motion.

3.1.3. Compact nature and depletion of hydration waters results in a higher modulus of elasticity

The importance of hydration water for elasticity of the elastin protein is well-known [42,43]. By examining the radial distribution function of water molecules around tropoelastin (Fig. S3A), we find two close hydration shells, one within 2.2 Å, representing water molecules involved in hydrogen bond formation with the protein, and the other between 2.2 Å and 3.2 Å, representing the secondary hydration shell of the protein. Compared with the control, the introduction of calcium ions decreases the number of hydration water molecules within the first two hydration shells (Fig. S2B (i)-(ii)). This result, along with an observed enhanced structural collapse of tropoelastin, may contribute to the significant increase in elastic modulus (Fig. 2A), where domain 19 is fixed, and domain 10 is pulled in the presence of increased calcium concentration, with starting conformation as shown in Fig. 2B (i). With more calcium ions present, it becomes increasingly harder to pull the molecule at the same strain. Notably, the phase-wise deformation patterns become more pronounced in the presence of higher calcium concentrations, as seen in the corresponding snapshots presented (Fig. 2B): elastic deformation from strain = 0 to 0.7 (Fig. 2B (i)-(ii)), as domain 10 is extended, then followed by a softening phase until strain = 1.16 (Fig. 2B (iii)); a stiffening phase from strain = 1.16 to 1.72 (Fig. 2B (iii)-(iv)), as domain 11 is extended, then followed by a short phase of softening until a strain of 2.3 (Fig. 2B (v)); elastic deformation from strain = 2.3 to 3.2, characterized by a very small slope (Fig. 2B (v)-(vi)), where domain 12 is about to be pulled out; from strain = 3.2 to 4.6, we observe a stiffening phase (Fig. 2B (vi)-(vii)), as domain 12 is extended, then followed by a softening phase until a strain = 8.6 (Fig. 2B (viii)); at strain = 8.6 to 19.5, there is another stiffening phase of the protein. Such distinct deformation patterns point to calcium-induced stiffness.

To examine the role of each domain in this phase-wise deformation pattern, we analyze dissociation profiles of protein-protein hydrogen bonds formed within each domain (Fig. S2C (i) -(x)). The number of hydrogen bonds formed by domain 10 is stable until strain = 11, suggesting its recurring role in resisting deformation until strain = 11. The number of hydrogen bonds formed by domain 11 is smaller yet also stable until strain = 13. The number of hydrogen bonds formed by domain 12 increases slightly until strain = 5.0, followed by a steady phase until strain = 16, also suggesting its involvement in modulating deformation. The number of hydrogen bonds formed by domain 14 shows a slight increase during initial deformation, followed by a decrease until strain = 4 and stabilization until strain = 8, indicating its role in resisting the pulling force during the initial deformation regime and in the phase from strain 4 to 8. Domain 15 shows a similar trend where the number of hydrogen bonds slightly increases before strain = 1.2, keeping steady until a large decrease at strain = 2.5, followed by another two steady states from strain = 2.5 to 4.8, and strains = 5.0 to 13.0, indicating its role in resisting deformation during these steady states.

Interestingly, compared with the dissociation profiles of hydrogen bonds of the control (Fig. S3B (i)-(x)), the presence of calcium ions encourages the formation of a larger number of more stable hydrogen bonds formed by each domain, especially in domains 10, 11, 12, 14, pointing to roles for calcium ions in stabilizing hydrogen bonds formed within the protein for increasing global molecular stiffness.

3.2. Glucose binding effects on structure and mechanical properties of elastin

3.2.1. Glucose exhibits affinity to residues different from those involved in the Maillard reaction

Structural variations and motion variability of WT tropoelastin in 1969 mM glucose were analyzed (Fig. 2). Prior to the formation of AGEs, proteins first undergo the Maillard reaction, where the free ε-amino groups of lysines or arginines react and link with the aldehyde group of C1 of open-ring sugar molecules [44,45]. More than 99% of glucose exists as a closed-ring conformation in aqueous solutions; while a minority, the open-ring conformation has generated discernable AGE crosslinks in substantially higher amounts than its low relative occupancy would suggest [46]. We hypothesized that glucose with the closed-ring conformation also has intrinsic propensity to interact with lysines and may be catalyzed into the open-ring conformation later, as proposed by Wang et al. [47].

We find several transient interactions between glucose and the protein, with three glucose molecules persistently binding three different pockets of tropoelastin, as detailed in the time-wise representative structures (Fig. 3A (i)). One pocket is surrounded by central domains, including 9, 10, 11, 16, 17 and 18 and its binding is stable during the whole simulation time; two pockets are trapped at the bridge and foot region, among domains 24, 28 and 29 and among domains 26-30, with a shorter contact time of 400 ns and 800 ns in total, respectively (Fig. 3A (ii)). Surprisingly, instead of contacting lysines and arginines involved in the Maillard

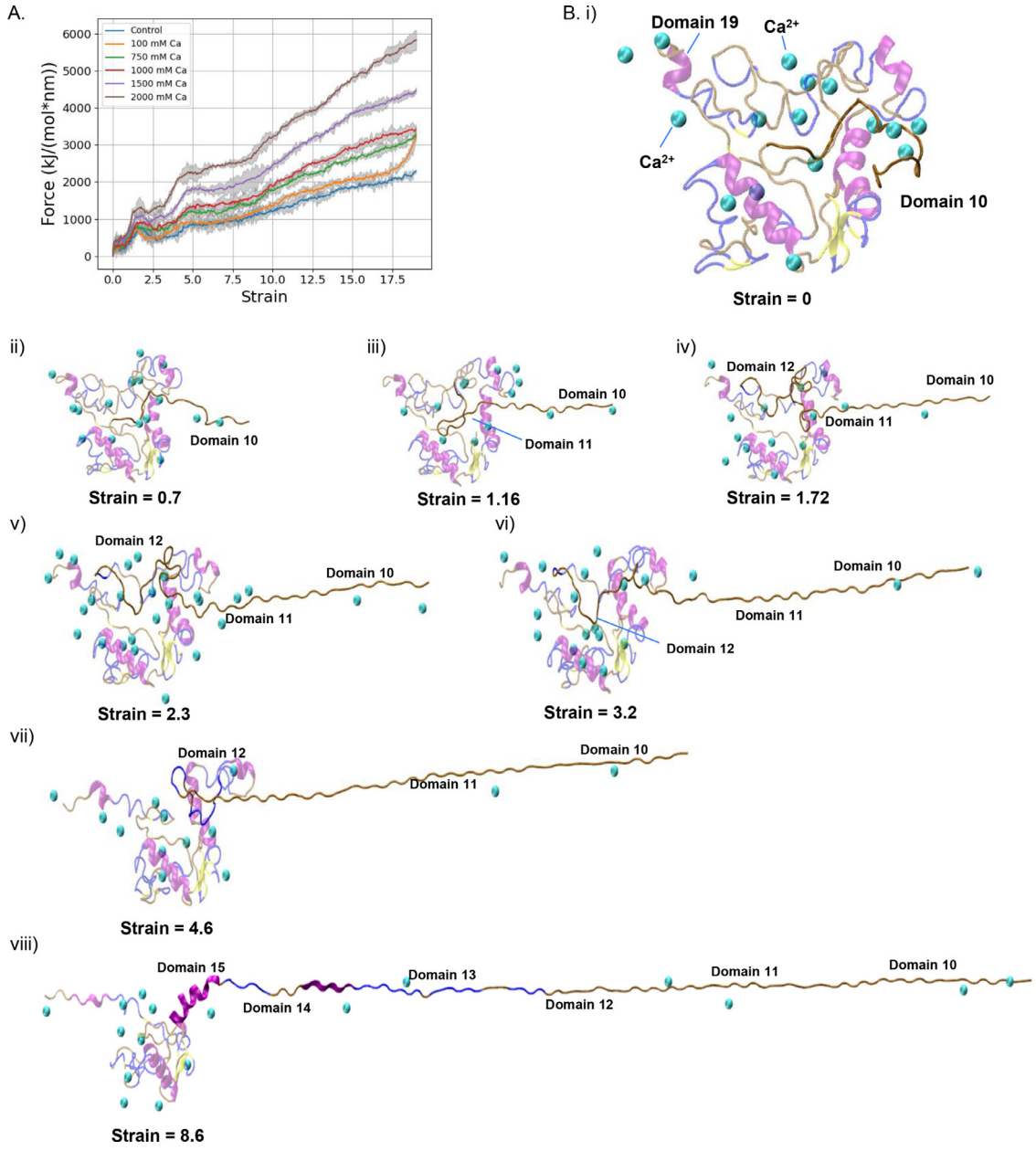

Fig. 2. Calcium effects on tropoelastin mechanics.
(A) Force vs strain curves in the presence of various concentrations of calcium.
(B) Snapshots of tensile tests at (i) Strain = 0, (ii) Strain = 0.7, (iii) Strain = 1.16, (iv) Strain = 1.72, (v) Strain = 2.3, (vi) Strain = 3.2, (vii) Strain = 4.6, (viii) Strain = 8.6, of tropoelastin + 1000 mM calcium ions. Domains about to be pulled are annotated and highlighted.

reaction, these glucose molecules show higher affinity to alanines and glycines, possibly due to their smaller steric hindrance that supports initial noncovalent binding with glucose, thereby further triggering mutorotation of glucose, and yielding a path for reactive, ring-opened glucose to be able to glycate tropoelastin [46].

3.2.2. Glucose binding disrupts ordered structure locally and globally

Contrary to the tendency of elastin to form ordered secondary structures by calcium binding, the interactions between glucose and elastin result in a higher percentage of coils locally in three persistent binding pockets, and a reduction in beta structures (Fig. S4A (i)-(iii)). Significant increase in coil content and decrease in both helices and beta structures are also observed globally (Fig. 3B), suggesting an increased propensity for the protein to assume a more disordered state in the presence of glucose.

These changes are induced by strong hydrogen bonding between tropoelastin and glucose, competing with hydrogen bonding within the protein as well as between protein and water. As shown in Fig. 3C (i)-(iii), fewer hydrogen bonds are identified within the protein and between tropoelastin and water in the presence of glucose. However, there is an increase in protein and non-protein hydrogen bonding, indicating the way by which glucose interacts with tropoelastin. Tropoelastin in the presence of glucose shows a tendency for structural dissociation, as presented in the time-wise representative structures (Fig. 3A (i)).

Salt bridges formed in the presence of glucose also exhibit different patterns compared to the control (Fig. 3D (i)-(ii)). The salt bridge between D72 and K78 is no longer stable; instead, a salt bridge between E345 and K289 from domain 17 emerges with a higher longevity. Since lysines of domain 17 are proposed to be

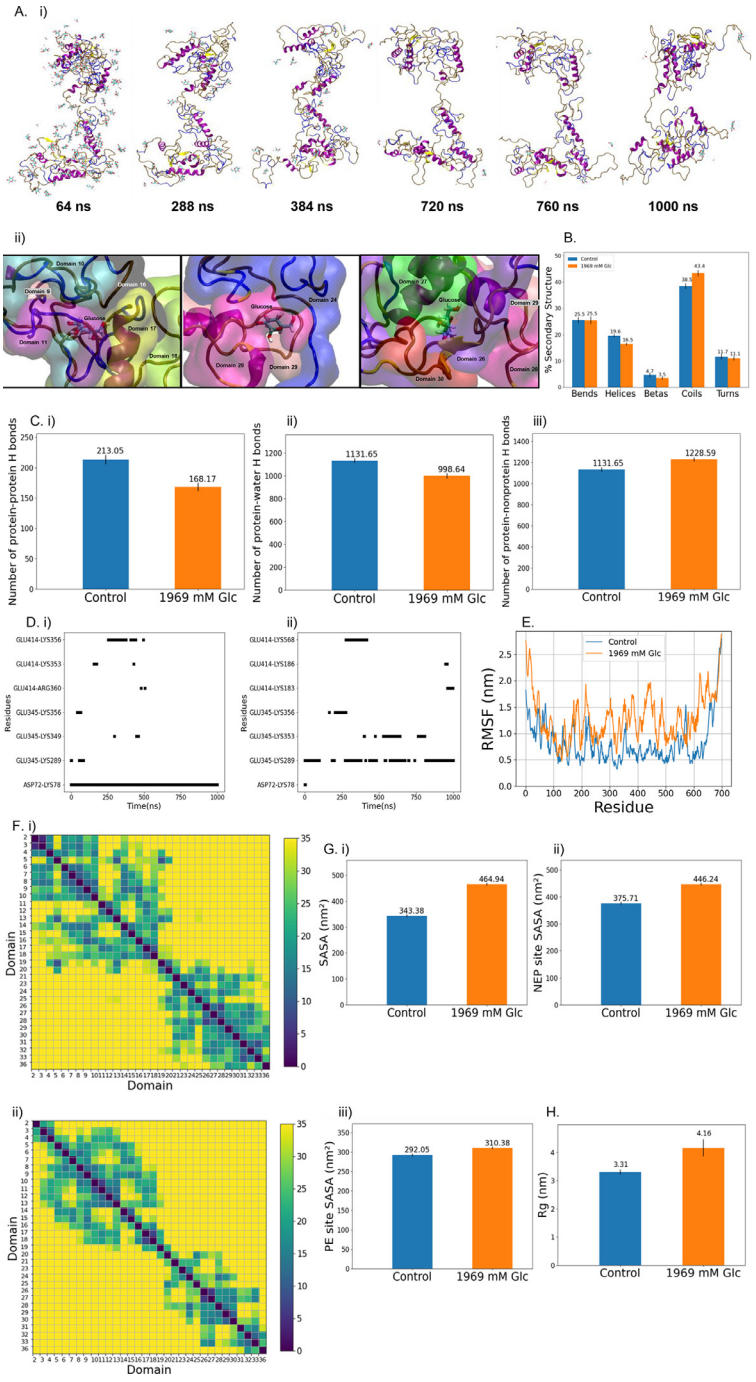

Fig. 3. Glucose effects on tropoelastin structure
(A, i) Representative structures of tropoelastin + 1969 mM glucose (ii) snapshots of three binding pockets.
(B) Global secondary structure of control and tropoelastin + 1969 mM glucose in the last 100 ns of simulation.
(C) Global hydrogen bonding of control and tropoelastin + 1969 mM glucose for (i) intramolecular bonding, (ii) bonding between protein and water and (iii) bonding between protein and non-protein in the last 100 ns of simulation.
(D) Salt bridge presence and longevity of (i) control and (ii) tropoelastin + 1969 mM glucose.
(E) Root mean square fluctuation (RMSF) of control and tropoelastin + 1969 mM glucose.
(F) Residue-wise contact maps with a cut-off distance of 35 A showing intramolecular interactions in (i) control and (ii) tropoelastin + 1969m M glucose in the last 100 ns of simulation.
(G) Solvent accessible surface area (SASA) of control and tropoelastin + 1969 mM glucose for (i) the whole molecule, (ii) cleavage sites by neprilysin and (iii) cleavage sites by pancreatic elastase in the last 100 ns of simulation.
(H) Radius of gyration (Rg) of control and tropoelastin + 1969 mM glucose in the last 100 ns of simulation.

highly involved in interactions with heparan sulfate [48] and integrin binding [49], the presence of this elongated salt bridge presence may alter these biological activities. There is also a new salt bridge detected between E414 and K568 from domain 27, suggesting a change in spatial arrangement of the foot region [2]. Overall, we find that glucose-tropoelastin hydrogen bonding causes the protein to adapt less ordered secondary structures and altered salt bridge patterns.

3.2.3. Glucose binding drives higher local and global molecular flexibility

As local structures are loosened in the presence of glucose, the protein also exhibits aberrantly higher local flexibility compared to the control (Fig. 3E). This structural dissociation effect brought about by the hydrogen bonding between glucose and the protein also alters global molecular motions. The folds near the N-terminus are disrupted, and domains 2-3 deviate from their original position, no longer in the vicinity of domains 6-10 compared to the control. The foot region also experiences large-scale expansion, especially in domains 31-36, where the protein is extended during the simulation time. Such altered protein dynamics precipitate fewer intramolecular contacts (Fig. 3F (ii)), a discernible increment in SASA (Fig. 3G (i)), and an enhanced Rg (Fig. 3H), implying potential reduction in intramolecular cross-links and lower capacity for aggregation.

3.2.4. Replacement of hydration water and viscosity conferred by glucose yields altered mechanical properties

We examine the number hydration waters within a shell radius of 2.2 Å and 3.2 Å, in the presence of glucose and in the control (Fig. S4B (i)-(ii)). The former shows a reduced number of hydration waters that can be attributed to competing hydrogen bonding between protein and glucose replacing interactions with water. This bonding behavior also influences the mechanical properties of tropoelastin (Fig. 4A)). With a higher concentration of glucose, the elastic modulus increases. The phase-wise deformation patterns observed in tropoelastin with 1969 mM glucose are more discernible compared to the control. The corresponding snapshots are presented in Fig. 4B: an elastic deformation phase from strain = 0 to 1.37 (Fig. 4B (i)-(ii)), where domain 10 and 11 are about to be pulled out, then followed by a softening phase until strain = 1.89 (Fig. 4B (iii)); from strain = 1.89 to 4.7, we observe a stiffening phase (Fig. 4B (iii)-(iv)), where domain 12 are 13 are about to be pulled out, then followed by a softening phase until strain = 4.9 (Fig. 4B (v)); from strain = 4.9 to 5.9, an elastic deformation phase characterized by a very small slope is observed (Fig. 4B (v)-(vi)), where domain 14 is about to be pulled out; from strain = 5.9 (Fig. 4B (vi)) to 19.5, a discernible stiffening phase is observed, where the rest of domains are deformed. We believe such distinct deformation patterns to be the consequence of hydrogen bonding between glucose and tropoelastin.

To examine the role each domain plays in this phase-wise deformation pattern, we also analyze dissociation profiles of hydrogen bonds formed within the protein by each domain, as shown Fig. S4C (i) -(x). Similar to the behavior in the presence of calcium ions, domain 10 of tropoelastin with 1969 mM glucose also shows hydrogen bonding numbers that diminish more quickly after strain = 10. Hydrogen bonding in domain 11 in 1969 mM glucose exhibits an ascending phase until strain = 3.7, keeps steady until strain = 5.0, and is followed by a short descending phase to strain = 6.2, increasing until strain = 7.0, then remaining stable until strain = 12.5. Domain 12 shows a similar pattern as in tropoelastin with 1000 mM calcium ions yet with a short descending phase after strain = 10. Hydrogen bonding by domain 13 shows interesting fluctuating phases that initially decrease until strain = 5.0, increasing until strain = 8.5, followed by a final descending phase. Domain 14 has a lower number of hydrogen bonds from start to end, but the tendency is similar to that of tropoelastin with 1000 mM calcium ions. These findings also suggest the supporting roles of domains 10-14 in resisting deformation; the earlier dissociation pattern compared to control and tropoelastin with 1000 mM calcium ions, however, suggests the increased elastic modulus and overall stiffness are not likely due to increased intramolecular bonding, but instead, is associated with intermolecular hydrogen bonding between glucose and protein.

3.3. Calcium and glucose coupling effects on structure and mechanical properties when calcium concentration dominates

3.3.1. The addition of glucose in the presence of calcium ions induces nonlinear changes within structural rearrangement and molecular motions

A gradient glucose concentration series of 62.5 mM, 123 mM, 185 mM and 246 mM is introduced to simulations with protein in the presence of 750 mM calcium ions (Fig. 5A (i)- (iv)). We find that tropoelastin exhibits varied structural changes as the glucose concentration increases. In tropoelastin with 62.5 mM glucose + 750 mM calcium (Fig. 5A (i)), the dissociation and the downward shift of the N-terminus are observed at the same time. However, instead of moving toward the C-terminus and folding with domain 32 via domains 18-19 as in the case of tropoelastin with only calcium, the N-terminus in tropoelastin with 62.5 mM glucose + 750 mM calcium presents a right-skewed bend, and domain 25 from the bridge region is displaced inwards from its original vertical position to a horizontal position, to “shoulder” the contracted N-terminus by supporting domains 12, 18 and 20.

In tropoelastin with 123 mM glucose + 750 mM calcium (Fig. 5A (ii)), the dissociation, the right-skewed bend and the downward shift of the N-terminus are also observed, but domain 25 is displaced outward from its original vertical position together with domains 24 and 28 in order to similarly shoulder the contracted N-terminus by supporting domains 11, 12, 18 and 20.

In tropoelastin with 185 mM glucose + 750 mM calcium (Fig. 5A (iii)), the dissociation effects by glucose dominate in its conformation at the beginning of the simulation, even if there is calcium binding and overall higher calcium concentration in the box. The loosened N-terminus also exhibits a right-skewed bend, moving towards the bridge region. Rearrangement of structures occurs in the bridge and foot region, where domain 25 shifts upwards to provide support along with domains 21, 23 and 24 for the receding upper domains 2-6, 10-12, and 20.

In tropoelastin with 246 mM glucose + 750 mM calcium (Fig. 5A (iv)), the dissociation effects by glucose are also discernible in the N-terminus; however, it stays stable and does not recede towards the foot region or the C-terminus. In the bridge region, the degree between domain 25 and domain 26 progressively decreases so that these two domains are aligned in an antiparallel manner. In the foot region, there is a noticeable shift of domain 29 that is displaced from a horizontal position to a tilted one.

Due to the heterogeneous nature of the structural reorganization patterns induced by calcium and glucose coupling effects, distinctly different intramolecular contact maps for these four conditions are expected (Fig. 5B (i)- (iv)). Among these conditions, tropoelastin with 185 mM glucose + 750 mM calcium undergoes the most significant structural rearrangement, where most of its N-terminus collapses and shifts towards the bridge and foot regions. Therefore, it exhibits the most elevated local fluctuation (Fig. S5A) and the smallest Rg (Fig. S5B). A nonlinear tendency in SASA of the whole molecule, SASA of neprilysin (NEP) cleavage sites and pancreatic elastase (PE) cleavage sites are also observed (Fig. 5C (i)- (iii)); however, compared to SASA of the whole molecule and

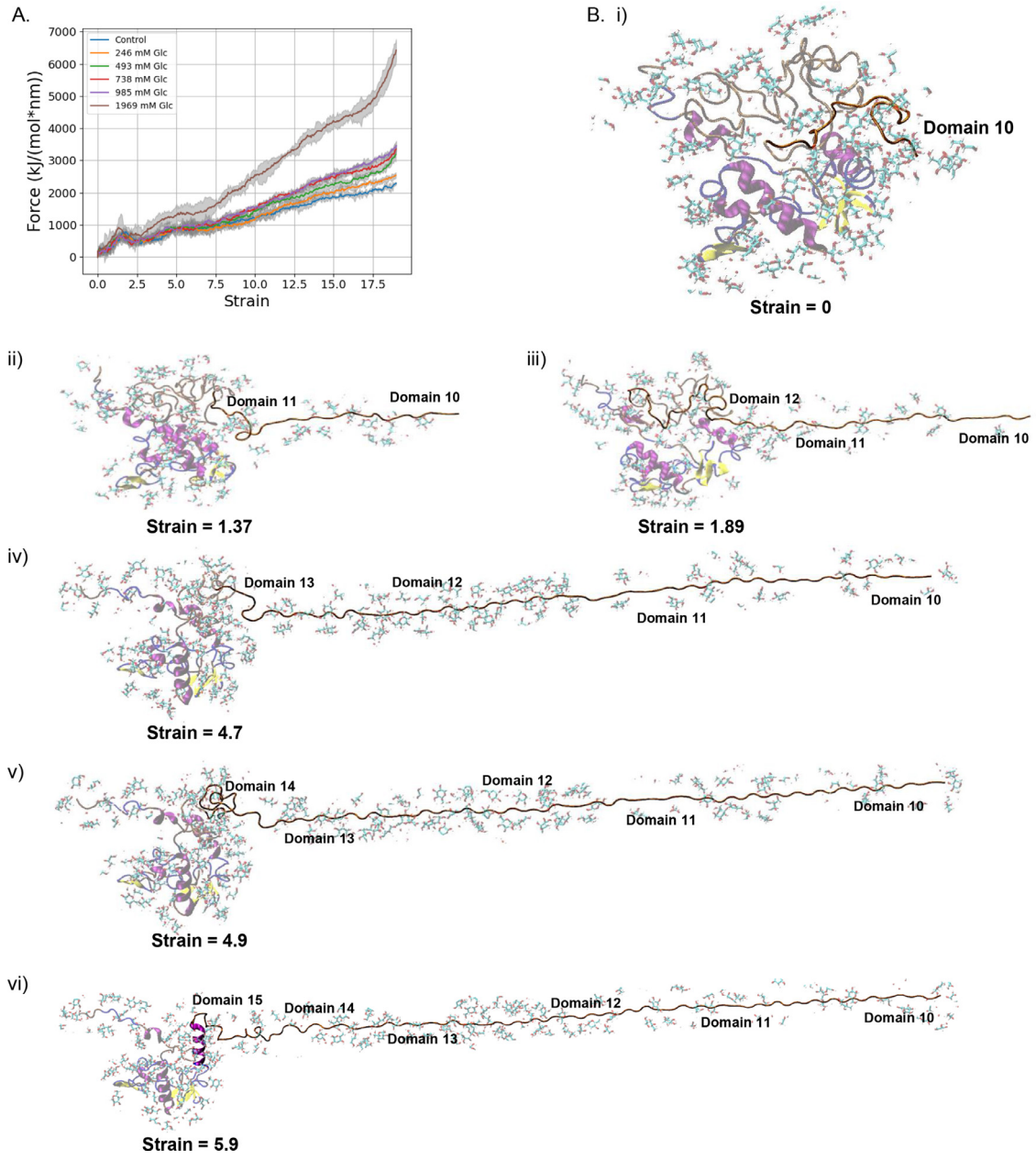

Fig. 4. Glucose effects on tropoelastin mechanics.
(A) Force vs strain curves in the presence of various concentrations of glucose.
(B) Snapshots of tensile tests at (i) Strain = 0, (ii) Strain = 1.37, (iii) Strain = 1.89, (iv) Strain = 4.7, (v) Strain = 4.9, (vi) Strain = 5.9, of tropoelastin + 1969 mM glucose. Domains about to be pulled are annotated and highlighted.

Rg, SASA of enzyme-targeted sites show a different tendency over the range of glucose concentrations, with a slight decrement with ascending glucose concentration from 62.5 mM to 123 mM, and an increased tendency displayed as glucose concentration increases further. However, the values of Rg and SASA of the whole molecule reduce with ascending glucose concentration from 62.5 mM to 185 mM and thereafter they increase. Despite its compact structure (i.e. smallest radius of gyration compared to other cases considered), the SASA value for NEP and PE of tropoelastin with 185 mM glucose + 750 mM calcium suggests that it does not have the least exposure towards enzymatic degradation. We infer that the small Rg of tropoelastin with 185 mM glucose + 750 mM calcium does not necessarily decrease the hindrance to cleavage sites of enzymes; instead, more exposure of these sites can occur due to the dissociation and expansion in its N-terminus, which may encourage elastase binding.

3.3.2. The addition of glucose in the presence of calcium ions induces nonlinear alterations in protein structure

As shown in time-wise representative structures in Fig. 5A (i)-(iv), all four conditions have the same four persistent calcium binding sites, D72, E345, E414 and K698 as seen in tropoelastin with only calcium. Notably, each binding site interacts with one calcium ion except E414 in tropoelastin with 123 mM + 750 mM calcium, where there are two calcium ions bound to E414. The binding of glucose in these conditions is found to be relatively transient, and no recurring binding is identified.

Although the hydrogen bonding between tropoelastin and glucose overall increases as the glucose concentration increases (Fig. 5D (iii)), we observe a nonlinearity of tendency in the number of protein-protein hydrogen bonds and protein-water hydrogen bonds (Fig. 5D (i)-(ii)). Such nonlinearity can be attributed to the heterogeneous structural reorganization in the presence of coupled

glucose and calcium, which alters the accessible distribution of nitrogen and oxygen atoms involved in hydrogen bonding.

The persistent salt bridge formed in the control between D72 and K78 still has a lower occupancy under the four tested conditions (Fig. 5E (i)-(iv)); however, the increment of glucose concentration promotes the bridge between E345 in domain 19 and K289 in domain 17, with the same tendency in tropoelastin with only glucose. Notably, we find a unique persistent salt bridge between E345 in domain 19 and K286 in domain 17 that strengthens the bridge region, in tropoelastin with 246 mM glucose + 750 mM calcium, which may explain why the N-terminus does not undergo collapse only under this condition compared to the other three conditions.

We find a nonlinear tendency in the distribution of secondary structure changes as the glucose concentration increases (Fig. 5F). Tropoelastin with 123 mM + 750 mM calcium and tropoelastin with 185 mM glucose + 750 mM calcium show slightly higher bend content compared with control and the other two conditions; only tropoelastin with 123 mM glucose + 750 mM calcium tends to form more helices compared with the other three conditions and control. Only tropoelastin with 246 mM glucose + 750 mM calcium has higher β-structure content than control, and the other three conditions exhibit β-structure content uncorrelated to glucose concentration. All conditions except tropoelastin with 123 mM glucose + 750 mM calcium have a similar coil content compared to the control. None of these four conditions show a concentration-related trend relative to turn content, where tropoelastin with 62.5 mM glucose + 750 mM calcium exhibits the higher turn content, while the other three conditions increase slightly as the glucose concentrations grows. Overall, we find that the heterogeneity of structural rearrangement due to the coupling effects of glucose and calcium yields nonlinear variations in hydrogen bonding, salt bridge formation and secondary structure as glucose concentration increases.

3.3.3. The addition of glucose in the presence of calcium ions induces linear alterations in mechanical profiles

Hydration water profiles also display a heterogeneous tendency under different conditions (Fig. S5C (i)-(ii)). As the glucose concentration increases from 62.5 mM to 246 mM in the presence of 750 mM calcium, an increase of elastic modulus suggesting increased stiffness, though not discernible among 62.5 mM, 123 mM, 185 mM (Fig. 5G), is observed. These results suggest that calcium ions play a dominant role in imparting stiffness in this case, and glucose also has some effects at a high concentration.

3.4. Calcium and glucose coupling effects on structure and mechanical properties when glucose concentration dominates

3.4.1. The addition of calcium in the presence of glucose induces nonlinear alterations in structural rearrangement and molecular motions

A gradient calcium concentration series of 100 mM, 200 mM, 300 mM and 400 mM is introduced in the presence of 738 mM glucose. As seen in the previous case study, when calcium concentration is fixed and glucose concentration is varied, tropoelastin displays heterogeneous conformational changes as the calcium concentration goes up (Fig. 6A (i)-(iv)).

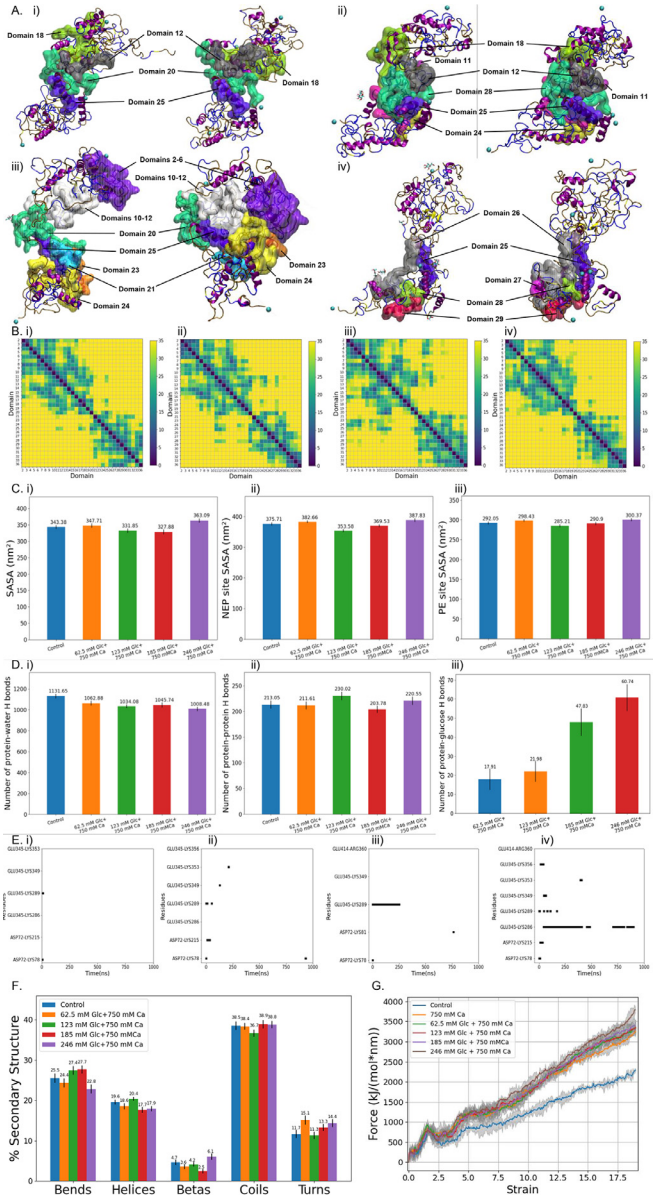

Fig. 5. Calcium and glucose coupling effects on tropoelastin structure and mechanics when calcium concentration is fixed at 750 mM.
(A) Representative structures of (i) tropoelastin with 62.5 mM glucose and 750 mM calcium, (ii) tropoelastin with 123 mM glucose and 750 mM calcium, (iii) tropoelastin with 185 mM glucose and 750 mM calcium, and (iv) tropoelastin with 246 mM glucose and 750 mM calcium.
(B) Residue-wise contact maps with a cut-off distance of 35 A showing intramolecular interactions in (i) tropoelastin with 62.5 mM glucose and 750 mM calcium, (ii) tropoelastin with 123 mM glucose and 750 mM calcium, (iii) tropoelastin with 185 mM glucose and 750 mM calcium, and (iv) tropoelastin with 246 mM glucose and 750 mM calcium in the last 100 ns of simulation.
(C) Solvent accessible surface area (SASA) in the control and tropoelastin with 62.5 mM glucose and 750 mM calcium, 123 mM glucose and 750 mM calcium, 185 mM glucose and 750 mM calcium, 246 mM glucose and 750 mM calcium for (i) the whole molecule, (ii) cleavage sites by neprilysin and (iii) cleavage sites by pancreatic elastase in the last 100 ns of simulation.
(D) Global hydrogen bonding in the control and tropoelastin with 62.5 mM glucose and 750 mM calcium, 123 mM glucose and 750 mM calcium, 185 mM glucose and 750 mM calcium, 246 mM glucose and 750 mM calcium for (i) intramolecular bonding, (ii) bonding between protein and water, (iii) bonding between protein and glucose in the last 100 ns of simulation (no glucose in the control).
(E) Salt bridge presence and longevity within (i) tropoelastin with 62.5 mM glucose and 750 mM calcium, (ii) tropoelastin with 123 mM glucose and 750 mM calcium, (iii) tropoelastin with 185 mM glucose and 750 mM calcium, and (iv) tropoelastin with 246 mM glucose and 750 mM calcium.
(F) Global secondary structure within the control and tropoelastin with 62.5 mM glucose and 750 mM calcium, 123 mM glucose and 750 mM calcium, 185 mM glucose and 750 mM calcium, 246 mM glucose and 750 mM calcium in the last 100 ns of simulation.
(G) Mechanical profiles of the control and tropoelastin with 750 mM calcium, 62.5 mM glucose and 750 mM calcium, 123 mM glucose and 750 mM calcium, 185 mM glucose and 750 mM calcium, 246 mM glucose and 750 mM calcium.

In tropoelastin with 738 mM glucose + 100 mM calcium (Fig. 6A (i)), evident dissociation of the N-terminus is observed. As shown in time-wise representative structure snapshots (Fig. 6A (i)-(iv)), the loosened N-terminus rearranges downwards. Rearrangement is also observed in the foot region, and domains proximal to the C-terminus, domains 30-36, displace significantly from their original positions and shift upwards in the vicinity of the collapsed domains 16-18. Domain 25 shifts inwards to a horizontal position to support the collapsed domains 12, 17 and 20.

In tropoelastin with 738 mM glucose + 200 mM calcium (Fig. 6A (ii)), the protein conformation is completely disrupted, rendering a loosely formed structure. A structural pattern of multiple layers of helices appears, where helices from domains 27, 29 and 31 align together at the foot to stabilize it; helices from domains 23 and 25 shift upward from their original position and coordinate with domain 21 to support the altered central region; the coils and bends from domains 18-20 shift upwards, so that domain 17 is found against the dissociated N-terminus, right above the layer formed by domains 21, 23 and 25.

In tropoelastin with 738 mM glucose + 300 mM calcium (Fig. 6A (iii)), in addition to the dissociation of the N-terminus, rearrangement of the hinge region and the foot region also takes places, where domains 21 and 23 shift downwards to the foot region along with helices from domains 25 and 26. A coordination of 6 helices in total from domains 21, 23, 25, 26, 27, 29, 31 located in the original hinge, bridge and foot region is characterized at the end of simulation time.

In tropoelastin with 738 mM glucose + 400 mM calcium (Fig. 6A (iv)), domains 25 is found to move away from its original position and shift inwards. Together with domains 21 and 23, it is tethered against the dissociated and collapsed upper regions of the protein, directly interacting with domains 7, 19 and 20.

Due to the heterogeneous conformations identified in response to calcium and glucose coupling effects, different intramolecular contact maps for these four conditions are expected (Fig. 6B (i)- (iv)). Among these conditions, tropoelastin with 738 mM glucose + 200 mM calcium has the largest local fluctuation around domains 18-20, corresponding to their structural rearrangement (Fig. S5D). Both tropoelastin with 738 mM glucose + 200 mM calcium and tropoelastin with 738 mM glucose + 400 mM calcium have substantial local fluctuation around domains 21, 23 and 24, corresponding to their upward shift to support upper collapsed regions (Fig. S5D).

Tropoelastin with 738 mM glucose + 300 mM calcium exhibits the largest Rg (Fig. S5E), consistent with its conformation at the end of the simulation time featuring less extent of collapse, whereas tropoelastin with 738 mM glucose + 100 mM calcium displays the smallest Rg, possibly due to its upward movement of the C-terminus.

A nonlinear tendency in SASA of the whole molecule, SASA of NEP cleavage sites and PE cleavage sites are also observed (Fig. 6C (i)- (iii)); however, compared with Rg values, SASA values show heterogeneous trends over the four conditions. Tropoelastin with 738 mM glucose + 300 mM calcium presents the smallest SASA whereas the largest Rg. This result is probably due to the highest hydrogen bonding between protein and glucose as shown in Fig. 6D (iii).

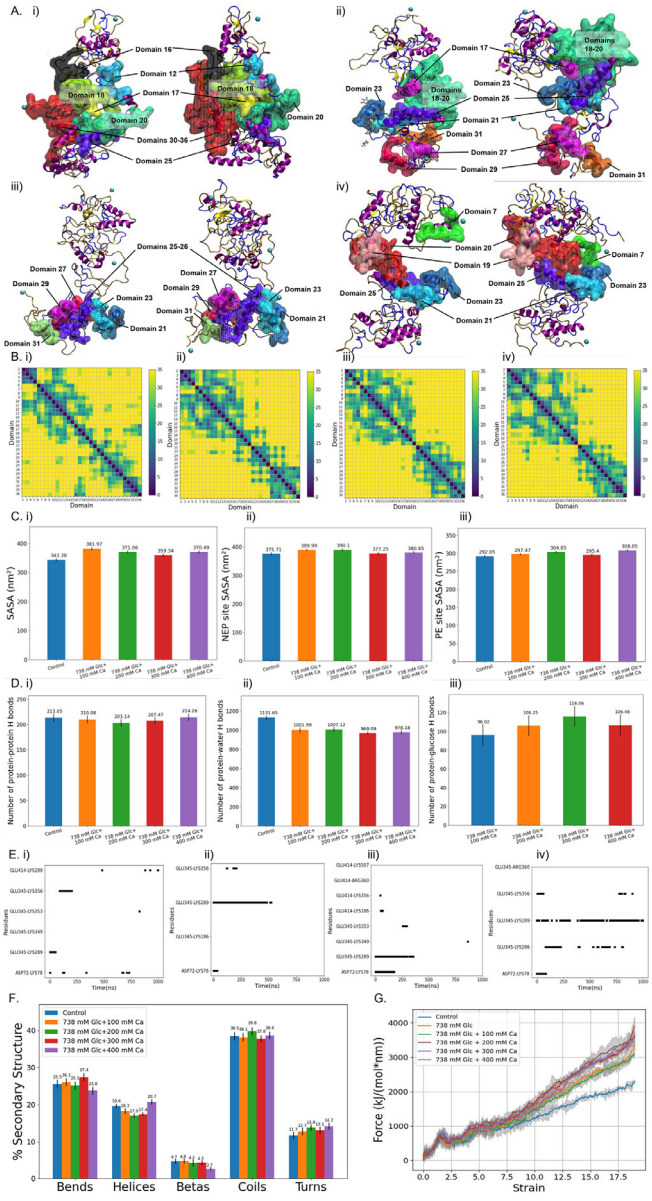

Fig. 6. Calcium and glucose coupling effects on tropoelastin structure and mechanics when glucose concentration is fixed at 738 mM.

(A) Representative structures of (i) tropoelastin with 100 mM calcium and 738 mM glucose, (ii) tropoelastin with 200 mM calcium and 738 mM glucose, (iii) tropoelastin with 300 mM calcium and 738 mM glucose, and (iv) tropoelastin with 400 mM calcium and 738 mM glucose.

(B) Residue-wise contact maps with a cut-off distance of 35 A showing intramolecular interactions in (i) tropoelastin with 100 mM calcium and 738 mM glucose, (ii) tropoelastin with 200 mM calcium and 738 mM glucose, (iii) tropoelastin with 300 mM calcium and 738 mM glucose, and (iv) tropoelastin with 400 mM calcium and 738 mM glucose in the last 100 ns of simulation.

(C) Solvent accessible surface area (SASA) in the control and tropoelastin with 100 mM calcium and 738 mM glucose, 200 mM calcium and 738 mM glucose, 300 mM calcium and 738 mM glucose, 400 mM calcium and 738 mM glucose, for (i) the whole molecule, (ii) cleavage sites by neprilysin and (iii) cleavage sites by pancreatic elastase in the last 100 ns of simulation.

(D) Global hydrogen bonding within the control and tropoelastin with 100 mM calcium and 738 mM glucose, 200 mM calcium and 738 mM glucose, 300 mM calcium and 738 mM glucose, and 400 mM calcium and 738 mM glucose for (i) intramolecular bonding, (ii) bonding between protein and water, (iii) bonding between protein and glucose in the last 100 ns of simulation (no glucose in the control).

(E) Salt bridge presence and longevity in (i) tropoelastin with 100 mM calcium and 738 mM glucose, (ii) tropoelastin with 200 mM calcium and 738 mM glucose, (iii) tropoelastin with 300 mM calcium and 738 mM glucose, and (iv) tropoelastin with 400 mM calcium and 738 mM glucose.

(F) Global secondary structure in the control and tropoelastin with 100 mM calcium and 738 mM glucose, with 200 mM calcium and 738 mM glucose, with 300 mM calcium and 738 mM glucose, and with 400 mM calcium and 738 mM glucose in the last 100 ns of simulation.

(G) Mechanical profiles of control and tropoelastin with 738 mM glucose, 100 mM calcium and 738 mM glucose, 200 mM calcium and 738 mM glucose, 300 mM calcium and 738 mM glucose, 400 mM calcium and 738 mM glucose.

3.4.2. Calcium in the presence of glucose induces nonlinear alterations in both local and global structure

As shown in time-wise representative structures in Fig. 6A (i)-(iv), all four conditions have four persistent calcium binding sites as in tropoelastin with only calcium, except in tropoelastin with 738 mM glucose + 400 mM calcium, where its E345 in domain 19 does not have recurring calcium binding sites. The binding of glucose in these conditions is found to be relatively transient, and no recurring binding is identified.

The hydrogen bonding between protein and glucose is found to increase as the calcium concentration increases from 100 mM to 300 mM (Fig. 6D (iii)), and decreases when calcium concentration reaches 400 mM, suggesting a competing mechanism of interaction in the presence of higher calcium concentration. Fewer protein-protein hydrogen bonds and more protein-water hydrogen bonds form in tropoelastin with 738 mM glucose + 200 mM (Fig. 6D (i)-(ii)), likely because its loosely formed multilayer structure by alignment of helices separates tropoelastin into smaller disconnected regions, among which fewer intramolecular hydrogen bonds are able to form but has sufficient surface accessibility for glucose and water interaction.

The persistent salt bridge between D72 and K78 formed in the control is similarly shorter-lived in the four tested conditions (Fig. 6E (i)-(iv)). Interestingly, the increment of calcium ion concentration promotes the salt bridge between E345 in domain 19 and K289 in domain 17, similar to the behavior of tropoelastin with only glucose. In tropoelastin with 738 mM glucose + 400 mM calcium, this salt bridge has highest longevity among all other conditions, possibly due to the absence of calcium binding to E345. All the conformations in these four conditions do not undergo significant collapse as we find in the four cases, which can be attributed to the dominating glucose concentration.

We find irregular distributions of secondary structure as the calcium concentration grows (Fig. 6F). Again, this heterogeneity, including within hydrogen bonding patterns, salt bridge formation and secondary structures, suggests that tropoelastin has a high number of degrees of freedom, and its conformations can vary significantly in response to minor changes in the surrounding environment.

3.4.3. The addition of calcium in the presence of glucose induces linear alterations in mechanical profiles

As the hydration water number in both hydration shells shows a nearly linear decrement as the calcium concentration increases (Fig. S5F (i)-(ii)), we would expect there to be a clear linear change in mechanical profiles. However, when glucose concentration dominates, the addition of calcium only shows significant difference between tropoelastin with 738 mM glucose + 100 mM calcium and tropoelastin with 738 mM glucose + 200 mM calcium, and a slight difference between tropoelastin with 738 mM glucose + 200 mM calcium and tropoelastin with 738 mM glucose + 400 mM calcium (Fig. 6G). It is possible that changes due to the relatively small increase in calcium concentration are not discernible in steered MD simulations, and glucose may block calcium from interacting with the protein, as observed in the case of MD simulation of tropoelastin with 738 mM glucose + 400 mM calcium.

4. Discussion

4.1. Possible role of calcium binding as an inhibitor in elastase degradation, cell interactions, cross-linking and self-assembly

The binding effects of calcium on tropoelastin conformation, dynamic behavior and mechanical properties are illustrated in Figs. 1 and 2. Calcium binding-induced structural collapse results in a compact global structure and increased stiffness, with likely downstream implications to tropoelastin's propensity for elastase degradation, cell interactions, cross-linking and self-assembly.

To predict the impacts of observed structural variability on enzymatic interactions with elastin, we compare the solvent accessible surface area (SASA) of cleavage sites within tropoelastin with and without calcium ions, associated with neprilysin (NEP), an enzyme also known as skin fibroblast-derived elastase [50], and pancreatic elastase (PE) [51] specifically targeting elastin. It has been reported that the up-regulation of these enzymes occurs during aging and is related to the degradation of the elastic fiber network [50]. As depicted in Fig. 1H (ii) and (iii), tropoelastin with calcium ions exhibits lower accessibility of the cleavage sites for both degradation enzymes, suggesting an inhibitor role of calcium binding. Globally, the reduction in overall SASA (Fig. 1H (ii)) is not only likely to inhibit enzymatic crosslinking but may also play a role in inhibiting coacervation and downstream fiber assembly. Meanwhile, with a decrement in SASA in elastase cleavage sites, calcium-bound elastin, with impaired participation in assembly, is less likely to be decomposed. The identified calcium binding sites may therefore act as nucleation sites where calcification accumulates during aging.

Our results also suggest that calcium ions further interact with specific functional regions of tropoelastin, likely disrupting their functions. As previously reported in the literature, intramolecular salt bridges formed between negatively charged residues and proximal lysines and arginines play a positive role in stabilizing the N-terminus by D72, hinge regions by E345, and bridge regions by E414 [25,52,53]. The introduction of calcium disrupts all the pre-existing salt bridges. Thereby, a rearrangement of tropoelastin's structural conformations is observed, as expected: local secondary structures are changed, the N-terminus destabilizes, and domains 18 and 19 shift downward and contact with domain 32.

Additionally, domain 10 has been reported to associate with domains 19 and 25 in another tropoelastin molecule via canonical demosine and lysinonorleucine cross-links [54], and to undergo a head-to-tail multi-molecular assembly, as proposed by Baldock et al. [55]. Since domain 32 shifts between domains 19 and 25, we infer that calcium-bound tropoelastin molecules are likely unable to undergo this multi-molecular assembly.

Calcium ions also bind to K698 because it is located at the C-terminus and thus has a free carboxylate group. Calcium binding decreases the mobility of this residue (Fig. 1B). Since the C-terminus is chiefly involved in cell adhesion during elastogenesis and incorporation into elastic fibers [27,56–59], mediating the initiation or acceleration of the assembly process [60], we expect that the functionality of K698 will be negatively impacted due to its impaired fluctuation induced by calcium binding.

4.2. Possible role of glucose as an enhancer in elastase degradation, other enzymatic reactions, and biological processes

The binding effects of glucose on tropoelastin conformation, dynamic behavior and mechanical properties are illustrated in Figs. 3 and 4. Glucose binding-induced structural dissociation results in loosely formed global structures, while substantial hydrogen bonding between tropoelastin and glucose yields stiffening in the mechanical response. Based on the structural and mechanical changes observed in the presence of glucose, we infer that glucose binding also likely plays an important role in elastase degradation, other enzymatic reactions, and biological processes. Similar to the case of calcium, we compare the SASA of cleavage sites by NEP and PE between the control and tropoelastin with glucose. As depicted in Fig. 3G (ii) and (iii), tropoelastin with glucose exhibits higher solvent accessible surface areas of cleavage sites associated with both degradation enzymes, suggesting that interactions with glucose expose cleavage sites, facilitating degradation by enzymes.

These results correspond to previous reports that glycation may be associated with an increase in the susceptibility towards enzymatic degradation [8]. As the interactions between concentrated glucose and tropoelastin tend to unravel the protein, it is reasonable to conclude that glucose binding may also enhance other enzymatic reactions by exposing the active sites. Notably, even if the closed-ring glucose molecules in our simulations do not show significant affinity to the lysines involved in the Maillard reaction, it is possible that these glucose molecules induce the reaction in another way: glucose with the closed-ring conformation unfolds the protein, non-covalently binding to the pockets we have identified, undergoing mutorotation to open rings, so that glucose with the open-ring conformation can thereby interact with lysine residues with minimal steric hindrance [46].

We expect the presence of glucose to also hinder normal assembly processes of tropoelastin. As glucose tends to extend the tropoelastin molecule, candidate crosslinking lysine residues are shifted to more distant positions with respect to crosslinking partners, which may impede intramolecular cross-linking. Domains 10, 19 and 25 also shift from their canonical positions, potentially hampering head-to-tail assembly. The markedly enhanced flexibility in the foot region and C-terminus (Fig. 2E) can also likely impact cell-mediated interactions and fiber assembly.

4.3. Implications of glucose and calcium coupling effects in altering normal biological processes

The introduction of different combinations of glucose and calcium to tropoelastin yields nonlinear variations in protein conformations, since these solvents invoke divergent changes to the molecule's structural rearrangement, namely, structural collapse by calcium, and structural dissociation by glucose. While the properties of protein conformation, e.g. SASA, Rg and hydrogen bonding, do not show a clear linear tendency as glucose concentration grows when calcium concentration dominates, the dynamic behavior of tropoelastin suggests a correlation between structural collapse and glucose concentration. Under glucose concentration ranging from 62.5 mM to 185 mM, tropoelastin displays a pronounced structural collapse (Fig. 5A (i)-(iii)). At 246 mM glucose, the protein structure stabilizes, suggesting that at this concentration glucose binding effects compete with calcium binding effects. When glucose concentration dominates, protein dynamics do not exhibit a correlation over a range of calcium concentrations, possibly due to a higher number of conformational degrees of freedom that arise from the molecular flexibility promoted by glucose binding.

Among these different combinations of glucose and calcium, we observe that domain 25 from the bridge region plays a central role in supporting the collapsed or loosened N-terminus and central domains by shifting upwards in both cases when calcium or glucose dominates. As revealed in previous studies, the bridge region is postulated to moderate elastic fiber assembly via association by coacervation and its vicinity to nearby cross-linking domains [61]. This observation implies an additional potential role of the bridge region in supporting the foot region and C-terminus. With a pronounced displacement of domain 25 to a position supporting the upper regions, the self-assembly behavior of tropoelastin with coupled glucose and calcium are expected to be negatively impacted, leading to potentially impaired coacervation, decreased head-to-tail multimer assembly, and ultimately compromised fiber assembly.

From a macroscopic perspective, our findings also provide insights into diseases of elastin of genetic origin. For instance, elastin gene deletions in Williams Syndrome result in reduced expression of functional elastin and an altered deposition of elastin in skin [62]. Given reports of occasional childhood hypercalcemia in Williams Syndrome [63], there are, nevertheless, contradictory observations of the phenotype of accompanied arterial stiffness, namely, a paradoxical reduction in arterial stiffness [64], and an increase in arterial stiffness [65,66]. Our findings may point to arterial recovery through reversible calcium binding, and support a general model where other calcium-binding molecules are needed to achieve persistent vascular calcium binding. It may also be that elastin attracts calcium through persistent binding, and that this persistence is locked in by resident calcium-binding proteins such as fibrillin-1. Overall, these studies have implications for uncontrolled, persistent hypercalcemia and hyperglycemia, where we hypothesize changes in biomechanics and adverse physiological consequences due to stiffening on a larger scale, particularly in the vasculature where functional elasticity is needed [67].

5. Conclusions

We perform atomistic classical MD simulations and steered MD simulations on tropoelastin in the presence of various concentrations of glucose and calcium ions. We find that both calcium ions and glucose can interact with tropoelastin molecules, altering their local structure, and thereby perturbing globular geometry, molecular motions, and mechanical properties, but by distinct molecular mechanisms. Overall, calcium binding enhances elastin's structural collapse, reducing elastin's flexibility, yielding a more ordered and rigid structure, with lower apparent susceptibility towards enzymatic degradation. Glucose binding dissociates ordered structure, enhancing elastin's flexibility and surface area accessible to solvent, which may also yield higher susceptibility to elastase degradation and may promote the Maillard reaction. Both molecular interactions disrupt the canonical structure of tropoelastin and increase the elastic modulus, which may in turn interrupt normal biological processes including cell interactions, cross-linking and self-assembly. We also find a nonlinear pattern in the changes that occur to tropoelastin conformations and molecular motions induced by glucose and calcium coupling effects. This is consistent with the model of tropoelastin as a highly sensitive protein to environmental change, due to a high number of degrees of freedom in the system. This understanding of the behavior of tropoelastin in these physiological environments has implications for the biomechanics of elastin biomaterials under these conditions, and provides a set of guidelines for the generation of novel materials to ameliorate these effects.

Declaration of Competing Interest

The authors declare no conflicts of interest.

Acknowledgements

This research was supported by the National Science Foundation, grant no. 2145759. This work utilized the Extreme Science and Engineering Discovery Environment (XSEDE), which is supported by National Science Foundation grant number ACI-1548562 (83). XSEDE resources Stampede 2 and Ranch at the Texas Advanced Computing Center and Bridges 2 at the Pittsburg Supercomputing Center through allocation TG-MCB180008 were used.

Supplementary materials

Supplementary material associated with this article can be found, in the online version, at doi:10.1016/j.actbio.2022.03.041.

References

[1] C.M. Kielty, M.J. Sherratt, C.A. Shuttleworth, Elastic fibres, J. Cell Sci. 115 (14) (2002) 2817–2828.

[2] J. Ozsvar, C. Yang, S.A. Cain, C. Baldock, A. Tarakanova, A.S. Weiss, Tropoelastin and elastin assembly, Front. Bioeng. Biotechnol. 9 (2021) 643110.
[3] L. Robert, A.M. Robert, T. Fulop, Rapid increase in human life expectancy: will it soon be limited by the aging of elastin? Biogerontology 9 (2) (2008) 119–133.
[4] L. Duca, S. Blaise, B. Romier, M. Laffargue, S. Gayral, H. El Btaouri, C. Kawecki, A. Guillot, L. Martiny, L. Debelle, P. Maurice, Matrix ageing and vascular impacts: focus on elastin fragmentation, Cardiovasc. Res. 110 (3) (2016) 298–308.
[5] O. Fritze, B. Romero, M. Schleicher, M.P. Jacob, D.Y. Oh, B. Starcher, K. Schenke-Layland, J. Bujan, U.A. Stock, Age-related changes in the elastic tissue of the human aorta, J. Vasc. Res. 49 (1) (2012) 77–86.
[6] N. Niederhoffer, I. Lartaud-Idjouadiene, P. Giummelly, C. Duvivier, R. Peslin, J. Atkinson, Calcification of medial elastic fibers and aortic elasticity, Hypertension 29 (1997) 999–1006.
[7] A.K. Baldwin, A. Simpson, R. Steer, S.A. Cain, C.M. Kielty, Elastic fibres in health and disease, Expert Rev. Mol. Med. 15 (2013) e8.
[8] A. Heinz, Elastic fibers during aging and disease, Ageing Res. Rev. 66 (2021) 101255.
[9] J.A. Beto, The role of calcium in human aging, Clin. Nutr. Res. 4 (1) (2015) 1–8.
[10] Y. Wang, S. Zeinali-Davarani, E.C. Davis, Y. Zhang, Effect of glucose on the biomechanical function of arterial elastin, J. Mech. Behav. Biomed. Mater. 49 (2015) 244–254.
[11] H.H. Dao, R. Essalihi, C. Bouvet, P. Moreau, Evolution and modulation of age-related medial elastocalcinosis: impact on large artery stiffness and isolated systolic hypertension, Cardiovasc. Res. 66 (2) (2005) 307–317.
[12] J.E. Wagenseil, R.P. Mecham, Elastin in large artery stiffness and hypertension, J. Cardiovasc. Transl. Res. 5 (2012) 264–273.
[13] C.L. Simpson, J.A. Mosier, N.R. Vyavahare, Osteoclast-mediated cell therapy as an attempt to treat elastin specific vascular calcification, Molecules 26 (2021) 3643.
[14] R.J. Elliott, L.T. McGrath, Calcification of the human thoracic aorta during aging, Calcif. Tissue Int. 54 (4) (1994) 268–273.
[15] S.Y. Yu, H.T. Blumenthal, The calcification of elastic fibers. I. Biochemical studies, J. Gerontol. 18 (1963) 119–126.
[16] L.K. Niskanen, M. Suhonen, O. Siitonen, J.M. Lehtinen, M.I. Uusitupa, Aortic and lower limb artery calcification in type 2 (non-insulin-dependent) diabetic patients and non-diabetic control subjects. A five year follow-up study, Atherosclerosis 84 (1) (1990) 61–71.
[17] W. Stanford, B.H. Thompson, R.M. Weiss, Coronary artery calcification: clinical significance and current methods of detection, AJR Am. J. Roentgenol. 161 (6) (1993) 1139–1146.
[18] M. Baumann, T. Richart, D. Sollinger, J. Pelisek, M. Roos, T. Kouznetsova, H.H. Eckstein, U. Heemann, J.A. Staessen, Association between carotid diameter and the advanced glycation endproduct Nε-Carboxymethyllysine (CML), Cardiovasc. Diabetol. 8 (2009).
[19] E. Yoshinaga, A. Kawada, K. Ono, E. Fujimoto, H. Wachi, S. Harumiya, R. Nagai, S. Tajima, N(ε)-(carboxymethyl)lysine modification of elastin alters its biological properties: implications for the accumulation of abnormal elastic fibers in actinic elastosis, J. Invest. Dermatol. 132 (2) (2012) 315–323.
[20] K. Mizutari, T. Ono, K. Ikeda, K. Kayashima, S. Horiuchi, Photo-enhanced modification of human skin elastin in actinic elastosis by N(epsilon)-(carboxymethyl)lysine, one of the glycoxidation products of the Maillard reaction, J. Invest. Dermatol. 108 (5) (1997) 797–802.
[21] D.M. Nathan, Long-term complications of diabetes mellitus, N. Engl. J. Med. 328 (23) (1993) 1676–1685.
[22] K. Janda, M. Krzanowski, M. Gajda, P. Dumnicka, E. Jasek, D. Fedak, A. Pietrzycka, M. Kuźniewski, J.A. Litwin, W. Sułowicz, Vascular effects of advanced glycation end-products: content of immunohistochemically detected AGEs in radial artery samples as a predictor for arterial calcification and cardiovascular risk in asymptomatic patients with chronic kidney disease, Dis. Markers 2015 (2015).
[23] N. Niederhoffer, I. Lartaud-Idjouadiene, P. Giummelly, C. Duvivier, R. Peslin, J. Atkinson, Calcification of medial elastic fibers and aortic elasticity, Hypertension 29 (4) (1997) 999–1006.
[24] I. Perrotta, E. Russo, C. Camastra, G. Filice, G. di Mizio, F. Colosimo, P. Ricci, S. Tripepi, A. Amorosi, F. Triumbari, G. Donato, New evidence for a critical role of elastin in calcification of native heart valves: immunohistochemical and ultrastructural study with literature review, Histopathology 59 (2011) 504–513.
[25] A. Tarakanova, G.C. Yeo, C. Baldock, A.S. Weiss, M.J. Buehler, Molecular model of human tropoelastin and implications of associated mutations, Proc. Nat. Acad. Sci. USA 115 (2018) 7338–7343.
[26] S.A. Hollingsworth, R.O. Dror, Molecular dynamics simulation for all, Neuron 99 (6) (2018) 1129–1143.
[27] A. Tarakanova, G.C. Yeo, C. Baldock, A.S. Weiss, M.J. Buehler, Tropoelastin is a flexible molecule that retains its canonical shape, Macromol. Biosci. 19 (2019).
[28] G.C. Yeo, A. Tarakanova, C. Baldock, S.G. Wise, M.J. Buehler, A.S. Weiss, Subtle balance of tropoelastin molecular shape and flexibility regulates dynamics and hierarchical assembly, Sci. Adv. 2 (2) (2016) e1501145.
[29] B. Hess, C. Kutzner, D. van der Spoel, E. Lindahl, GROMACS 4: algorithms for highly efficient, load-balanced, and scalable molecular simulation, J. Chem. Theory Comput. 4 (3) (2008) 435–447.
[30] J. Huang, S. Rauscher, G. Nawrocki, T. Ran, M. Feig, B.L. de Groot, H. Grubmuller, A.D. MacKerell Jr., CHARMM36m: an improved force field for folded and intrinsically disordered proteins, Nat. Methods 14 (1) (2017) 71–73.
[31] W.L. Jorgensen, J. Chandrasekhar, J.D. Madura, R.W. Impey, M.L. Klein, Comparison of simple potential functions for simulating liquid water, J. Chem. Phys. 79 (2) (1983) 926–935.
[32] U. Essmann, L. Perera, M.L. Berkowitz, T. Darden, H. Lee, L.G. Pedersen, A smooth particle mesh Ewald method, J. Chem. Phys. 103 (19) (1995) 8577.
[33] G. Bussi, D. Donadio, M. Parrinello, Canonical sampling through velocity rescaling, J. Chem. Phys. 126 (2007).
[34] M.R. Parrinello, Polymorphic Transitions in Single Crystals: a new molecular dynamics method, J. Appl. Phys. 52 (1981) 7182–7190.
[35] R.W. Hockney, S.P. Goel, J. Eastwood, Quiet high resolution computer models of a plasma, J. Comp. Phys. 14 (1974) 148–158.
[36] B. Hess, H. Bekker, H.J. Berendsen, J.G. Fraaije, LINCS: a linear constraint solver for molecular simulations, J. Comp.Chem. 18 (12) (1997) 1463–1472.
[37] W.G. Hoover, Canonical dynamics: equilibrium phase-space distributions, Phys. Rev. A Gen. Phys. 31 (3) (1985) 1695–1697.
[38] W. Humphrey, A. Dalke, K. Schulten, VMD: visual molecular dynamics, J. Mol. Graph. 14 (1) (1996) 33–38 27-8.
[39] W. Kabsch, C. Sander, Dictionary of protein secondary structure: pattern recognition of hydrogen-bonded and geometrical features, Biopolymers 22 (12) (1983) 2577–2637.
[40] R. Gowers, M. Linke, J. Barnoud, T. Reddy, M. Melo, S. Seyler, O. Beckstein, MDAnalysis: a python package for the rapid analysis of molecular dynamics simulations, in: Proceedings of the 15th Python in Science Conference, 2016, pp. 98–105.
[41] N. Michaud-Agrawal, E.J. Denning, T.B. Woolf, O. Beckstein, MDAnalysis: a toolkit for the analysis of molecular dynamics simulations, J. Comput. Chem. 32 (10) (2011) 2319–2327.
[42] M.A. Lillie, J.M. Gosline, The effects of hydration on the dynamic mechanical properties of elastin, Biopolymers 29 (8–9) (1990) 1147–1160.
[43] Y. Wang, J. Hahn, Y. Zhang, Mechanical properties of arterial elastin with water loss, J. Biomech. Eng. 140 (2018).
[44] D.R. Sell, V.M. Monnier, Molecular basis of arterial stiffening: role of glycation-a mini-review, Gerontology (2012) 227–237.
[45] W.T. Yoshikazu Yonei, Masayuki Yagi, Photoaging and glycation of elastin: effect on skin, Glycative Stress Res. 2 (4) (2015) 182–190.
[46] S.L. Clark, A.E. Santin, P.A. Bryant, R. Holman, K.J. Rodnick, The initial noncovalent binding of glucose to human hemoglobin in nonenzymatic glycation, Glycobiology 23 (11) (2013) 1250–1259.
[47] Y. Wang, H. Yu, X. Shi, Z. Luo, D. Lin, M. Huang, Structural mechanism of ring-opening reaction of glucose by human serum albumin, J. Biol. Chem. 288 (2013) 15980.
[48] P. Lee, G.C. Yeo, A.S. Weiss, A cell adhesive peptide from tropoelastin promotes sequential cell attachment and spreading via distinct receptors, FEBS J. 284 (14) (2017) 2216–2230.
[49] P. Lee, D.V. Bax, M.M. Bilek, A.S. Weiss, A novel cell adhesion region in tropoelastin mediates attachment to integrin alphaVbeta5, J. Biol. Chem. 289 (3) (2014) 1467–1477.
[50] A.C. Mora Huertas, C.E.H. Schmelzer, C. Luise, W. Sippl, M. Pietzsch, W. Hoehenwarter, A. Heinz, Degradation of tropoelastin and skin elastin by neprilysin, Biochimie 146 (2018) 73–78.
[51] A.C. Mora Huertas, C.E.H. Schmelzer, W. Hoehenwarter, F. Heyroth, A. Heinz, Molecular-level insights into aging processes of skin elastin, Biochimie 128-129 (2016) 163–173.
[52] G.C. Yeo, C. Baldock, S.G. Wise, A.S. Weiss, A negatively charged residue stabilizes the tropoelastin N-terminal region for elastic fiber assembly, J. Biol. Chem. 289 (50) (2014) 34815–34826.
[53] G.C. Yeo, C. Baldock, S.G. Wise, A.S. Weiss, Targeted modulation of tropoelastin structure and assembly, ACS Biomater. Sci. Eng. 3 (2017) 2832–2844.
[54] P. Brown-Augsburger, C. Tisdale, T. Broekelmann, C. Sloan, R.P. Mecham, Identification of an elastin cross-linking domain that joins three peptide chains. Possible role in nucleated assembly, J. Biol. Chem. 270 (30) (1995) 17778–17783.
[55] C. Baldock, A.F. Oberhauser, L. Ma, D. Lammie, V. Siegler, S.M. Mithieux, Y. Tu, J.Y.H. Chow, F. Suleman, M. Malfois, S. Rogers, L. Guo, T.C. Irving, T.J. Wess, A.S. Weiss, Shape of tropoelastin, the highly extensible protein that controls human tissue elasticity, Proc. Natl. Acad. Sci. 108 (2011) 4322–4327.
[56] T.J. Broekelmann, B.A. Kozel, H. Ishibashi, C.C. Werneck, F.W. Keeley, L. Zhang, R.P. Mecham, Tropoelastin interacts with cell-surface glycosaminoglycans via its COOH-terminal domain *, J. Biol. Chem. 280 (2005) 40939–40947.
[57] S.G. Wise, A.S. Weiss, Tropoelastin, Int. J. Biochem. Cell Biol. 41 (3) (2009) 494–497.
[58] S.G. Wise, G.C. Yeo, M.A. Hiob, J. Rnjak-Kovacina, D.L. Kaplan, M.K.C. Ng, A.S. Weiss, Tropoelastin: a versatile, bioactive assembly module, Acta Biomater. 10 (4) (2014) 1532–1541.
[59] P. Brown-Augsburger, T. Broekelmann, J. Rosenbloom, R.P. Mecham, Functional domains on elastin and microfibril-associated glycoprotein involved in elastic fibre assembly, Biochem. J. 318 (Pt 1) (1996) 149–155.
[60] W.H. Kozel, Davis. BA, Mecham.RP. EC, Domains in tropoelastin that mediate elastin depositionin vitro and in vivo, J. Biol. Chem. 278 (20) (2003) 18491–18498.
[61] G.C. Yeo, C. Baldock, A. Tuukkanen, M. Roessle, L.B. Dyksterhuis, S.G. Wise, J. Matthews, S.M. Mithieux, A.S. Weiss, D.A. Tirrell, Tropoelastin bridge region positions the cell-interactive C terminus and contributes to elastic fiber assembly, Proc. Nat. Acad. Sci. USA 109 (8) (2012) 2878–2883.
[62] Z. Urban, S. Peyrol, H. Plauchu, M.T. Zabot, M. Lebwohl, K. Schilling, M. Green, C.D. Boyd, K. Csiszar, Elastin gene deletions in Williams syndrome patients result in altered deposition of elastic fibers in skin and a subclinical dermal phenotype, Pediatr. Dermatol. 17 (1) (2000) 12–20.
[63] T.L. Stanley, A. Leong, B.R. Pober, Growth, body composition, and endocrine issues in Williams syndrome, Curr. Opin. Endocrinol. Diabetes Obes. 28 (1) (2021) 64–74.

[64] P. Lacolley, P. Boutouyrie, M. Glukhova, J.M. Daniel Lamaziere, P.F. Plouin, P. Bruneval, P. Vuong, P. Corvol, S. Laurent, Disruption of the elastin gene in adult Williams syndrome is accompanied by a paradoxical reduction in arterial stiffness, Clin. Sci. (Lond.) 103 (1) (2002) 21–29.
[65] B.A. Kozel, J.R. Danback, J.L. Waxler, R.H. Knutsen, L. de Las Fuentes, G.S. Reusz, E. Kis, A.B. Bhatt, B.R. Pober, Williams syndrome predisposes to vascular stiffness modified by antihypertensive use and copy number changes in NCF1, Hypertension 63 (1) (2014) 74–79.
[66] C.M. Halabi, T.J. Broekelmann, R.H. Knutsen, L. Ye, R.P. Mecham, B.A. Kozel, Chronic antihypertensive treatment improves pulse pressure but not large artery mechanics in a mouse model of congenital vascular stiffness, Am. J. Physiol. Heart Circ. Physiol. 309 (5) (2015) H1008–H1016.
[67] B. Park, Y.J. Lee, Borderline high serum calcium levels are associated with arterial stiffness and 10-year cardiovascular disease risk determined by Framingham risk score, J. Clin. Hypertens. (Greenwich) 21 (5) (2019) 668–673.